Letters

Modulation of Bidirectional AC/DC Converters Based on Half-Bridge Direct-Matrix Structure

Ngoc Dat Dao, *Student Member, IEEE*, and Dong-Choon Lee, *Senior Member, IEEE*

***Abstract*—This letter proposes a half-bridge bidirectional isolated matrix-based ac/dc converter for compact ac/dc power conversion applications. The converter can control not only the dc voltage or current, but also the power factor of the ac current with a single conversion stage, which helps to achieve a higher power density with a lower complexity. The converter operates with zero-voltage switching or zero-current switching in all switches. Hence, the switching frequency of the converter can be increased higher, leading to smaller passive components. Besides the simple circuit, the modulation scheme derived from time domain analyses is also easy to implement. The proposed topology has been verified by experimental results for a 2-kW SiC-based prototype. A high efficiency of 96.8% was achieved at a full load condition. The current total harmonic distortion (THD) is lower than 4% and the power density is 1.8 kW/dm^3.**

***Index Terms*—AC/DC converter, bidirectional switch, direct-matrix converter, power factor correction.**

I. Introduction

AC/DC converters have been employed for a wide range of applications such as data center power supplies, ac/dc distribution systems, battery chargers and energy storage systems. In some cases, an isolation transformer is needed for safety and high voltage ratio conversion. Conventional ac/dc converters consist of the rectifier stage with power factor correction (PFC) function and the isolated dc/dc stage [1], [2]. The PFC rectifier controls the dc-link voltage while regulating the ac current so that it has a low THD and in phase with the ac voltage. Usually, large-sized inductors with high inductance are used to filter the switching ripples in the ac current. With the constant dc-link voltage from the PFC rectifier, the dc/dc stage generates an isolated voltage through a transformer. Due to the two-stage structure, these ac/dc converters have low efficiency, high complexity, large boost inductor, and bulky dc-link electrolytic capacitor.

The efficiency can be improved by using single-stage ac/dc topologies, which consists of a full wave active rectifier and a dual active bridge (DAB) converter [3]–[5]. Instead of diodes, active switches are utilized in the rectifier to enable bidirectional power flow and to reduce the conduction losses. These switches operate at the ac frequency, so the switching losses are lower than the PFC rectifier in two-stage ac/dc converters. Rather than bulky boost inductors and large capacitors, only small high-frequency capacitors are employed at the rectifier output. The DAB converter plays a main role in the single-stage ac/dc converter, which is responsible for controlling both the output dc voltage and the ac current.

The line rectifier can be integrated into the DAB by utilizing bidirectional switches as seen in matrix converters [6]–[9]. The key advantage of these matrix ac/dc converters is that the power losses in the ac side are distributed equally between switches. Nonresonance or resonance operation modes can be utilized for the DAB converters.

To further reduce the complexity of the ac/dc converter, in this letter, a half-bridge direct-matrix-based ac/dc converter is proposed, which also has a single-stage power conversion and a capability of bidirectional power transfer. By employing the half-bridge structure on both ac and dc sides, the reliability and power density can be increased compared with those of converters using the full-bridge structure. A current-sensorless modulation scheme is developed to control the ac current with unity power factor and low THD. In addition, all switches are turned ON with ZCS or ZVS over the full range of the ac voltage and a wide range of load. The performance of the proposed ac/dc converter has been verified with a 2-kW SiC-based prototype. A high efficiency of 96.8% at rated condition and current THD lower than 4% are achieved. The initial idea of the proposed converter has been presented in [10], but detailed analyses and experimental results have not been added.

II. Topology and Operation Principle

A. Converter Configuration

The circuit diagram of the proposed ac/dc converter is illustrated in Fig. 1. On the primary side, there is a half-bridge comprising two bidirectional switches and two capacitors. A small inductor $L_{\rm ac}$ is connected to the primary half-bridge to filter the input current so that low-ripple current waveforms can be achieved. With high switching frequency, the value and size of this inductor can be reduced.

Manuscript received March 18, 2020; revised April 16, 2020 and May 6, 2020; accepted May 9, 2020. Date of publication May 13, 2020; date of current version July 31, 2020. This work was supported by the National Research Foundation of Korea under Grant NRF-2017R1A2A2A05069629 funded by the Korea Government (MSIT). *(Corresponding author: Dong-Choon Lee.)*

The authors are with the Department of Electrical Engineering, Yeungnam University, Gyeongbuk 38541, South Korea (e-mail: daongocdat@gmail.com; dclee@yu.ac.kr).

Color versions of one or more of the figures in this article are available online at https://ieeexplore.ieee.org.

Digital Object Identifier 10.1109/TPEL.2020.2994776

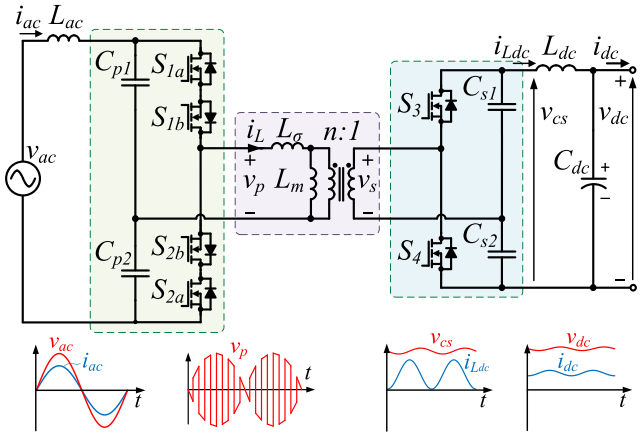

Fig. 1. Proposed single-stage half-bridge matrix-based ac/dc converter.

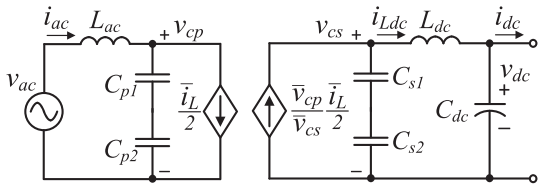

Fig. 2. Average model of the proposed converter.

On the secondary side, a half-bridge with two switches and two capacitors is used to regulate the ac current and the dc voltage. Like C_{p1} and C_{p2}, the capacitors C_{s1} and C_{s2} on the secondary side are not used for energy storage. Instead, they are designed with low capacitance and low parasitic resistance for filtering high-frequency high-pulse currents. However, if the capacitance values are too small, they will resonate with the transformer inductances. Since the power of a single-phase ac source contains double-fundamental frequency component, $L_{\rm dc}$ and $C_{\rm dc}$ are added to reduce the second-order ripple in the output power and voltage.

From the line voltage, the half-bridge on the ac side yields a high-frequency pulsed voltage, which is transferred to the secondary side through a high-frequency transformer. The transformer turn ratio is *n:1*. The transformer magnetizing and leakage inductances are denoted by L_σ and L_m, respectively. The transformer leakage inductance can be seen as an energy transfer element, which is a parameter to determine the maximum output power. On the other hand, the magnetizing inductance has no role in power transfer. Regardless of the power transfer direction, the converter can operate in boost or buck modes, where the dc output voltage referred to the ac side, $V'_{\rm dc} = nV_{\rm dc}$, can be lower or higher, respectively, than the maximum value of the ac voltage.

The simplified average model of the proposed converter is shown in Fig. 2. In the figure, $\bar{i}_L$ is the average transformer current over a half switching cycle on the ac side. Due to the power balance between two sides of the converter, the average transformer current on the dc side can be derived as $\bar{v}_{cp}\bar{i}_L/\bar{v}_{cs}$,

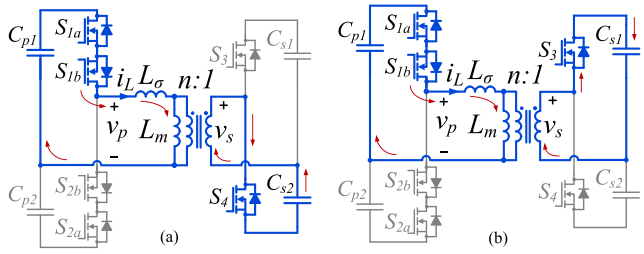

Fig. 3. Current paths during the positive-half cycle. (a) S_{1a}, S_{1b}, and S_4 are turned ON. (b) S_{1a}, S_{1b}, and S_3 are turned ON.

where $\bar{v}_{cp}$ and $\bar{v}_{cs}$ are the average values of v_{cp} and v_{cs}, respectively, in a switching period.

B. Operation Principle

On the ac side, the half-bridge circuit is operated at constant switching frequency with 50% duty cycle. When the ac voltage is positive, S_{1a} and S_{2a} are switched by complementary gating signals, whereas S_{1b} and S_{2b} are turned ON continuously. In contrast, if the ac voltage is negative, S_{1b} and S_{2b} are switched complementarily while S_{1a} and S_{2a} are turned ON.

The currents on ac and dc sides are regulated solely by the half-bridge on dc side. The transformer current is controlled by the duty cycles of S_3 and S_4 and the phase-shift between v_p and v_s. If the power flows from ac side to dc side, the converter operates similarly to the boost converter when $|v_{\rm ac}(t)| < v_{\rm dc}(t)$. Fig. 3 illustrates current paths in the converter during the positive-half cycle. At the beginning point of the switching cycle, when v_p is switched to $+/v_{\rm ac}|/2$, the switch S_4 is turned ON simultaneously. The current in transformer windings increases linearly while S_4 is turned ON. When S_4 is switched OFF, the transformer current flows through S_3 to the output capacitor C_{s1} and gradually decreases. After $T_s/2$, v_p is changed to $|v_{\rm ac}|/2$ and S_3 is turned ON. The same operation occurs, but the transformer current changes the direction. When $|v_{\rm ac}(t)| > v_{\rm dc}(t)$, the converter operates like the DAB converter.

C. Comparison Studies

The comparison between the proposed converter and the existing single-stage bidirectional isolated ac/dc converters has been made, which is listed in Table I. Among these converters, the proposed converter has the lowest number of switches and gate drivers, which makes the circuit board simpler. If low ON-resistance switches are used, high efficiency can be achieved as the same as that of full-bridge-based converters. In additions, the proposed converter operates at constant switching frequency and can achieve soft-switching over the entire operation range by a simple modulation scheme.

III. Time Domain Analysis and Control Method

Depending on the shape of the transformer current, two operating modes are identified as either discontinuous conduction mode (DCM) or continuous conduction mode (CCM).

TABLE I
COMPARISON OF COMPONENT COUNT, CONTROL METHOD AND EFFICIENCY AMONG SINGLE-STAGE AC/DC CONVERTERS

Topologies	Proposed half-bridge-based converter	Hybrid half-bridge & full-bridge converter [7], [8]	Full-bridge-based converter [6]	Full-bridge-based converter with line rectifier [3], [4]
Switches & gate drivers	6	8	12	12
Control variables	Duty ratio & single-phase-shift	Dual-phase-shift & switching frequency	Dual-phase-shift	Dual-phase-shift & triple-phase-shift
Full load efficiency	97%	97%	89%	96% [3], 98% [4]

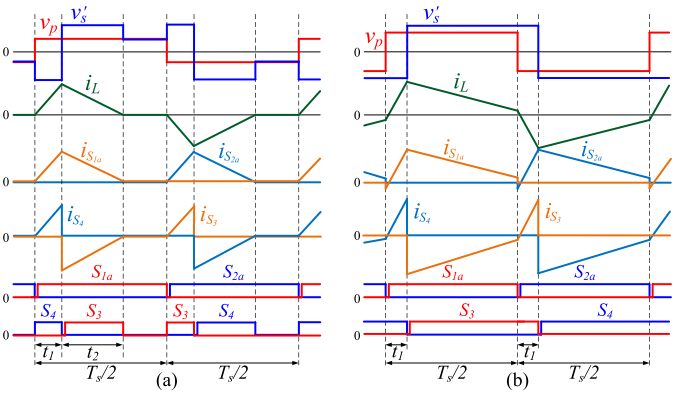

Fig. 4. Voltage and current waveforms in ac–dc operation. (a) Discontinuous conduction mode. (b) Continuous conduction mode.

Fig. 4 shows the waveforms during the positive period of the ac voltage with power flow direction from ac side to dc side. The secondary terminal voltage referred to the primary side is denoted by $v_s' = nv_s$. The DCM waveforms are illustrated in Fig. 4(a), where the transformer current increases linearly from zero and returns back to zero in half a switching cycle. The devices on the ac side are switched ON/OFF with ZCS. The switches S_3 and S_4 are turned ON with ZVS and ZCS, respectively. A higher switching loss occurs in S_4 than in S_3 since S_4 is turned OFF with high current whereas S_3 has ZCS turn-OFF. The CCM operation is shown in Fig. 4(b), where the current i_L is not zero at every switching instant. ZVS is achieved in all switches during CCM operation. In this case, the power is regulated by the phase-shift angle.

Since active switches are used for both ac and dc sides, the proposed converter allows bidirectional power transfer. From time domain analysis, modulation schemes are derived for both power flow directions.

A. Power Flows From AC Side to DC Side

Consider that C_{p1} and C_{p2} have sufficiently large capacitance so as to maintain their voltages during a switching period. The voltage drop on $L_{\rm ac}$ is also neglected since the impedance of $L_{\rm ac}$ at fundamental frequency is small. Thus, $v_{p1} = v_{p2} = v_{\rm ac}/2$. The bidirectional switches are controlled at a constant switching frequency with 50% duty cycle, so the primary terminal voltage can be expressed as follows:

$$v_p = v_{ab} = \begin{cases} v_{\rm ac}/2, & 0 < t < T_s/2 \\ -v_{\rm ac}/2, & T_s/2 < t < T_s. \end{cases} \tag{1}$$

C_{s1} and C_{s2} are also considered equal and enough large so that $v_{c1} = v_{c2} = v_{dc}/2$.

With a high value, the magnetizing inductance is not considered in this analysis for simplicity. The switching period begins when S_{1a}, S_{1b}, and S_4 are turned ON. During the turn-ON period t_1 of S_4, the transformer current increases linearly from zero to the maximum value $I_{L,\max}$, which is calculated as follows:

$$I_{L,\max} = d_1 T_s (v_{\rm ac} + nv_{\rm dc})/(4L_\sigma) \tag{2}$$

where $d_1 = 2t_1/T_s$ and d_1 varies from 0 to 1. When S_4 is OFF, the current flows through S_3 to the output and decreases with a slope

$$di_L/dt = (-v_{\rm ac} + nv_{\rm dc}) / (2L_\sigma). \tag{3}$$

Since the body diode has high voltage drop, S_3 needs to be turned ON during this interval to reduce the conduction loss. The duty ratio of S_3 for the period that i_L decreases from $I_{L,\max}$ to zero is calculated as follows:

$$d_2 = \frac{v_{\rm ac} + nv_{\rm dc}}{-v_{\rm ac} + nv_{\rm dc}} d_1. \tag{4}$$

The converter operates in DCM when $(d_1 + d_2) < 1$, which means

$$d_1 < 0.5 - v_{\rm ac}/(2nv_{\rm dc}). \tag{5}$$

The average transformer current over a half switching cycle can be obtained as follows:

$$I_{L,\rm DCM} = \frac{nv_{\rm dc}\,(v_{\rm ac} + nv_{\rm dc})}{4L_\sigma f_s\,(-v_{\rm ac} + nv_{\rm dc})} d_1^2. \tag{6}$$

When $d_1 > 0.5 - v_{\rm ac}/(2nv_{\rm dc})$, the converter operates in CCM. In this mode, S_3 and S_4 are switched complementarily with 50% duty cycle and the phase-shift ratio between v_p and v_s' is d_1. This operation is equivalent to that of the DAB converter with a single phase-shift modulation, thus the same equation can be utilized to calculate the transformer current as follows [11]:

$$I_{L,\rm CCM} = \frac{nv_{\rm dc}(d_1 - d_1^2)}{4L_\sigma f_s}. \tag{7}$$

From (6) and (7), the duty ratio d_1 can be calculated to produce a reference current I_L^* as follows:

$$d_1 = \begin{cases} \left[\dfrac{4L_\sigma f_s(-v_{\rm ac} + nv_{\rm dc})I_L^*}{nv_{\rm dc}(v_{\rm ac} + nv_{\rm dc})}\right]^{1/2}, & d_1 < d_b \\ \dfrac{1}{2} - \left(\dfrac{1}{4} - \dfrac{4L_\sigma f_s I_L^*}{nv_{\rm dc}}\right)^{1/2}, & d_1 > d_b \end{cases} \tag{8}$$

where $d_b = 0.5 - v_{\rm ac}/(2nv_{\rm dc})$ is the boundary between DCM and CCM operation.

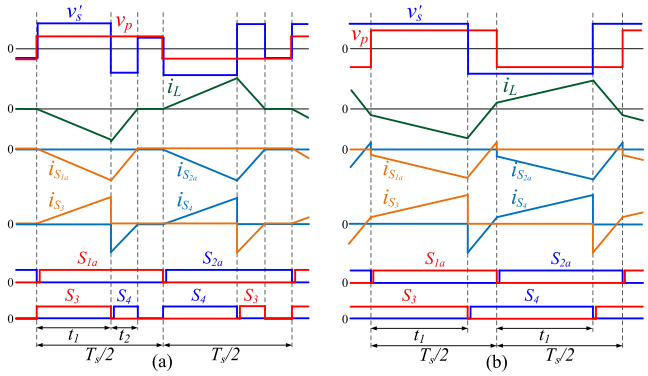

Fig. 5. Voltage and current waveforms in dc–ac operation. (a) Discontinuous conduction mode. (b) Continuous conduction mode.

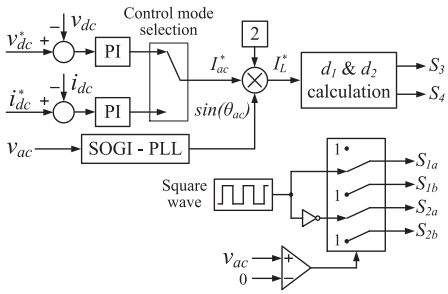

Fig. 6. Control block diagram for proposed ac/dc converter.

B. Power Flows From DC Side to AC Side

Fig. 5 shows the waveforms where the power direction is from dc side to ac side. S_3 will be turned ON during the ON states of S_{1a} and S_{1b}. Applying the same analysis method as in the previous section, the average transformer current in DCM can be derived as follows:

$$I_{L,\mathrm{DCM}} = \frac{nv_{\mathrm{dc}}\left(-v_{\mathrm{ac}} + nv_{\mathrm{dc}}\right)}{4L_\sigma f_s\left(v_{\mathrm{ac}} + nv_{\mathrm{dc}}\right)} d_1^2. \tag{9}$$

After S_3 is turned ON with the duty ratio d_1, S_4 will be turned ON for a period of t_2, which corresponds to the duty ratio d_2:

$$d_2 = d_1(-v_{\mathrm{ac}} + nv_{\mathrm{dc}})/(v_{\mathrm{ac}} + nv_{\mathrm{dc}}). \tag{10}$$

The boundary condition between DCM and CCM can be found as $d_b = 0.5 + v_{\mathrm{ac}}/(2nv_{\mathrm{dc}})$. Then, for a reference current I_L^*, the duty ratio d_1 can be calculated as follows:

$$d_1 = \begin{cases} \left[\dfrac{4L_\sigma f_s(v_{\mathrm{ac}} + nv_{\mathrm{dc}})I_L^*}{nv_{\mathrm{dc}}(-v_{\mathrm{ac}} + nv_{\mathrm{dc}})}\right]^{1/2}, & d_1 < d_b \\ \dfrac{1}{2} + \left(\dfrac{1}{4} - \dfrac{4L_\sigma f_s I_L^*}{nv_{\mathrm{dc}}}\right)^{1/2}, & d_1 > d_b. \end{cases} \tag{11}$$

C. Control Strategy

The control scheme for the proposed converter is illustrated in Fig. 6. The angle θ_{ac} of the AC voltage is detected by using the phase-locked loop. The dc voltage and current are regulated by proportional-integral (PI) controllers, where the control output is the magnitude of the ac current. Since the converter is composed of half-bridge modules, to generate the ac current, $i_{\mathrm{ac}}^* = I_{\mathrm{ac}}^* \sin(\theta_{\mathrm{ac}})$, the transformer current should be two times i_{ac}^*. Thus, the reference transformer current $I_L^* = 2I_{\mathrm{ac}}^* \sin(\theta_{\mathrm{ac}})$ is substituted into (8) or (11) along with the measured ac and dc voltages to obtain the required control variable d_1. Using d_1, d_2 is calculated by (4) or (10). In contrast, the ON/OFF conditions of switches on ac side are determined solely by the line voltage polarity.

The maximum transformer current occurs at the peak points of ac current. When power flows from the ac side to the dc side, the peak value of I_L is calculated as follows:

$$I_{L,\mathrm{pk}} = \left[nV_{\mathrm{dc}} + V_{\mathrm{ac}}(2d_{1,\mathrm{ac\_pk}} - 1)\right] / (8L_\sigma f_s) \tag{12}$$

where V_{dc} is the average dc output voltage, V_{ac} is the magnitude of the ac source, and $d_{1,\mathrm{ac-pk}}$ is calculated from (8) with $I_L^* = 2I_{\mathrm{ac,max}}$. For dc/dc operation, $I_{L,\mathrm{pk}}$ is obtained as follows:

$$I_{L,\mathrm{pk}} = \left[nV_{\mathrm{dc}} + V_{\mathrm{ac}}(1 - 2d_{1,\mathrm{ac\_pk}})\right] / (8L_\sigma f_s) \tag{13}$$

where $d_{1,\mathrm{ac\_pk}}$ is calculated from (11) with $I_L^* = 2I_{\mathrm{ac,max}}$.

As seen from (8) and (11), the maximum ac current that can be generated is $I_{\mathrm{ac,\,max}} = nv_{\mathrm{dc}}/(32L_\sigma f_s)$. So, L_σ or f_s can be reduced to increase the power capacity of the converter. The maximum average power that can be transferred between the ac side and the dc side is determined as follows:

$$P_{\mathrm{avg,max}} = 0.5V_{\mathrm{ac}}I_{\mathrm{ac,max}} = V_{\mathrm{ac}}nV_{\mathrm{dc}}/(64L_\sigma f_s). \tag{14}$$

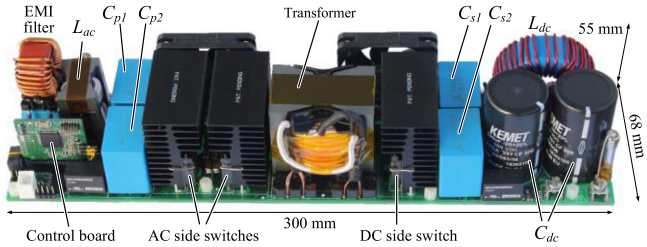

Fig. 7. 2 kW hardware prototype of the proposed ac/dc converter.

TABLE II
PARAMETERS OF 2-kW PROTOTYPE

Input voltage, V_{ac}	220 V 60 Hz	DC filter inductor, L_{dc}	300 μH
Output voltage, V_{dc}	400 V	DC filter capacitor, C_{dc}	300 μF
AC line inductor, L_{ac}	40 μH	Transf. turn ratio	1:1
AC side cap., C_{p1}, C_{p2}	10 μF	Transf. leakage ind., L_σ	23 μH
DC side cap., C_{s1}, C_{s2}	10 μF	Switching frequency	40 kHz

IV. EXPERIMENTAL RESULTS

A 2-kW prototype was built with a power density of 1.8 kW/dm^3 to validate the feasibility of the proposed ac/dc converter, as shown in Fig. 7. The parameters are given in Table II. The identical SiC MOSFETs are used for all the switches, of which model is SCT3030AL [12]. The device has the ON-resistance of 30 mΩ. The transformer is designed from the area product value, by an equation [13]

$$A_p = \frac{2P_{\max}10^4}{K_f K_u B_m J f_s} = \frac{2 \times 4000 \times 10^4}{4 \times 0.4 \times 0.2 \times 600 \times 40000} \approx 10.42\ \mathrm{cm}^4 \tag{15}$$

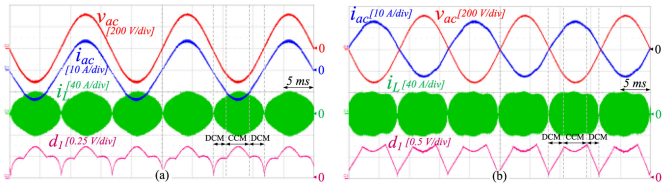

Fig. 8. Operating waveforms at rated condition. (a) Power flows from ac to dc. (b) Power flows from dc to ac.

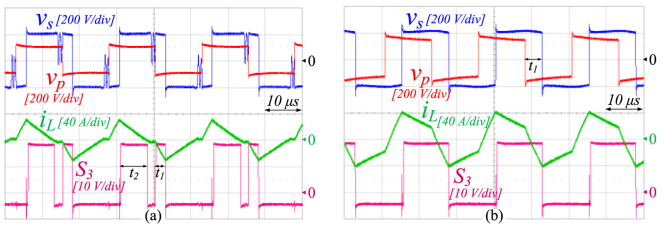

Fig. 9. Switching waveforms when power is transferred from ac to dc. (a) DCM operation. (b) CCM operation.

where $P_{\max}$ is the maximum power capacity, $K_f = 4$ is the waveform factor of square voltage, $K_u = 0.4$ is the utilization factor, $B_m = 0.2$ T is the maximum flux density, and $J = 600$ A/cm^2 is the current density. As a result, PQ50/50 ferrite core is selected, which has $A_p = 14.2\,\text{cm}^4$. The number of transformer turns on the ac side is calculated as follows:

$$N_{\text{ac}} = \frac{0.5V_{\text{ac,max}}10^4}{K_f B_m A_e f_s} = \frac{0.5 \times 220 \times \sqrt{2} \times 10^4}{4 \times 0.2 \times 3.32 \times 40000} \approx 14.6 \tag{16}$$

where $A_e = 3.32$ cm^2 is the effective magnetic cross section of the core. For implementation, $N_{\text{ac}} = 15$ is chosen. On the dc side, the turn number is also $N_{\text{dc}} = 15$ for 1:1 voltage ratio.

Fig. 8 shows the steady-state operation at the rated conditions. The output power is 2 kW and the input rms current is 9.4 A. The power is transferred from ac side to dc side in Fig. 8(a) and in the reverse direction in Fig. 8(b). The current THD values are 2.9% and 3.4% in Fig. 8(a) and (b), respectively. The power factor is unity in both cases. The shapes in the duty ratio d_1 are different between Fig. 8(a) and (b). The reason is that the converter operates in the boost mode to transfer power from ac side to dc side and in the buck mode for the reverse direction.

The peak current of transformer is 42 A. Compared with the full-bridge structure, the transformer current increases doubly in this half-bridge topology. Due to this disadvantage, low ON-resistance or parallel-connected devices should be used for high current applications. The converter operates in DCM when the line voltage is low or under light load conditions.

Figs. 9 and 10 show the switching waveforms in DCM and CCM with bidirectional power flow. During DCM, there are two duty ratios for the secondary-side switches. So, the equivalent switching frequency of S_3 and S_4 is 80 kHz. The deadtime between switches is 400 ns. In CCM, the transformer current is regulated by the phase-shift angle between the ac and dc terminal voltages.

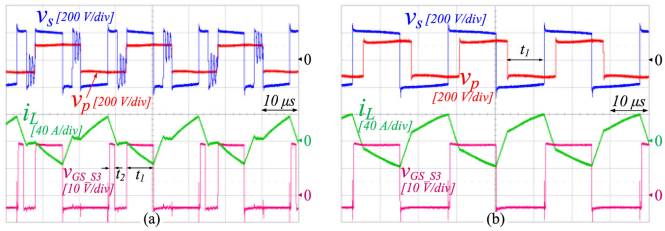

Fig. 10. Switching waveforms when power is transferred from dc to ac. (a) DCM operation. (b) CCM operation.

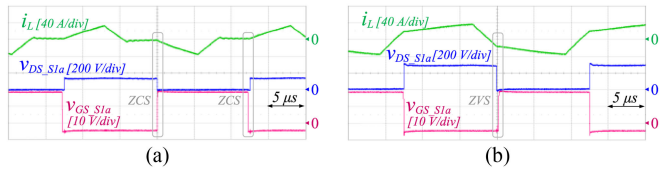

Fig. 11. Switching waveforms of S_{1a}. (a) DCM operation. (b) CCM operation.

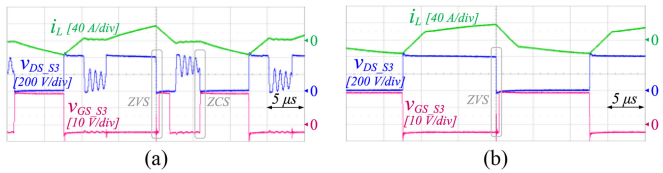

Fig. 12. Switching waveforms of S_3. (a) DCM operation. (b) CCM operation.

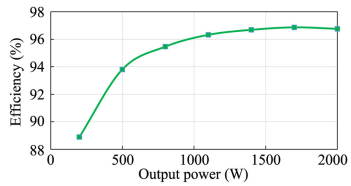

Fig. 13. Measured efficiency of the proposed converter.

Figs. 11 and 12 show the switching waveforms of S_{1a} and S_3, respectively. Due to the symmetry of the circuit, it can be concluded from the figures that all switches are turned on with either ZVS or ZCS.

Fig. 13 shows the measured efficiency of the proposed converter. With ZVS or ZCS turn-ON operation and low turn-OFF loss of SiC devices, the power losses of the converter are mainly determined by conduction losses. The efficiency is over 94% for output power higher than 500 W. The peak efficiency of 96.9% is achieved at 1700 W.

V. Conclusion

In this letter, a novel single-stage isolated ac/dc converter was proposed for bidirectional ac/dc conversion systems. The converter structure comprises two half-bridges and one high-frequency transformer. Bidirectional switches are employed in the ac side as seen in matrix converters. The main advantage of

the proposed converter topology is that it needs fewer semiconductor switches than other existing bidirectional isolated ac/dc converters. So, the circuit complexity is reduced. A simple control method has been developed to produce sinusoidal current waveforms with low THD and unity power factor. A 2-kW SiC-based prototype has been built and tested with a high efficiency of 96.8% at full load condition. The THD of grid current is lower than 4%.

REFERENCES

[1] A. Khaligh and S. Dusmez, "Comprehensive topological analysis of conductive and inductive charging solutions for plug-in electric vehicles," *IEEE Trans. Veh. Technol.*, vol. 61, no. 8, pp. 3475–3489, Oct. 2012.

[2] C. A. Gallo, F. L. Tofoli, J. Antonio, and C. Pinto, "Two stage isolated switch-mode power supply with high efficiency and high input power factor," *IEEE Trans. Ind. Electron.*, vol. 57, no. 11, pp. 3754–3766, Nov. 2010.

[3] J. Everts, F. Krismer, J. Van Den Keybus, J. Driesen, and J. W. Kolar, "Optimal ZVS modulation of single-phase single-stage bidirectional DAB AC-DC converters," *IEEE Trans. Power Electron.*, vol. 29, no. 8, pp. 3954–3970, Aug. 2014.

[4] J. Lu *et al.*, "A modular-designed three-phase high-efficiency high-power-density EV battery charger using dual/triple-phase-shift control," *IEEE Trans. Power Electron.*, vol. 33, no. 9, pp. 8091–8100, Sep. 2018.

[5] M. Kwon and S. Choi, "An electrolytic capacitorless bidirectional EV charger for V2G and V2H applications," *IEEE Trans. Power Electron.*, vol. 32, no. 9, pp. 6792–6799, Sep. 2017.

[6] N. D. Weise, G. Castelino, K. Basu, and N. Mohan, "A single-stage dual-active-bridge-based soft switched AC–DC converter with open-loop power factor correction and other advanced features," *IEEE Trans. Power Electron.*, vol. 29, no. 8, pp. 4007–4016, Aug. 2014.

[7] F. Jauch and J. Biela, "Combined phase-shift and frequency modulation of a dual-active-bridge AC–DC converter with PFC," *IEEE Trans. Power Electron.*, vol. 31, no. 12, pp. 8387–8397, Dec. 2016.

[8] T. Chen, R. Yu, Q. Huang, and A. Q. Huang, "A single-stage bidirectional dual-active-bridge AC-DC converter based on enhancement mode GaN power transistor," in *Proc. IEEE Appl. Power Electron. Conf. Exp.*, 2018, pp. 723–728.

[9] J. E. Huber, J. Böhler, D. Rothmund, and J. W. Kolar, "Analysis and cell-level experimental verification of a 25 kW all-SiC isolated front end 6.6 kV/400 V AC-DC solid-state transformer," *CPSS Trans. Power Electron. Appl.*, vol. 2, no. 2, pp. 140–148, 2017.

[10] N. D. Dao and D.-C. Lee, "Modulation and control of single-stage bidirectional isolated direct-matrix-based AC-DC converters," in *Proc. 10th Int. Conf. Power Electron. ECCE Asia*, 2019, pp. 2278–2283.

[11] N. D. Dao, D.-C. Lee, and Q. D. Phan, "High-efficiency SiC-based isolated three-port DC/DC converters for hybrid charging stations," *IEEE Trans. Power Electron.*, to be published, doi: 10.1109/TPEL.2020.2975124.

[12] SiC MOSFET. [Online]. Available: https://www.rohm.com/products/sic-power-devices/sic-mosfet/sct3030al-product, 2018.

[13] C. W. T. McLyman, *Transformer and Inductor Design Handbook*, 4th ed. New York, NY, USA, CRC Press, 2011.